THE ASTROPHYSICAL JOURNAL, 501:699–709, 1998 July 10

VLA OBSERVATIONS OF CARBON RADIO RECOMBINATION LINES TOWARD THE H II REGION COMPLEX S88B

GUIDO GARAY
Departamento de Astronomía, Universidad de Chile, Casilla 36-D, Santiago, Chile
YOLANDA GÓMEZ AND SUSANA LIZANO
Instituto de Astronomía, UNAM, Apartado Postal 70-264, 04510 México, D.F., Mexico
AND
ROBERT L. BROWN
National Radio Astronomy Observatory, 520 Edgemont Road, Charlottesville, VA 22903
Received 1997 November 5; accepted 1998 February 17

ABSTRACT

We present high angular resolution VLA observations of the C92α, C110α, and C166α radio recombination lines of carbon from the region of massive star formation known as S88B. The observations reveal that the carbon emission arises from two distinct components that are intimately associated with the compact (S88B2) and cometary (S88B1) regions of ionized gas within the complex. The brighter carbon component has an angular size of $\sim 6''.6$, an average line-center velocity of 21.0 ± 0.5 km s^{-1}, and an average line width of 5.1 ± 1.0 km s^{-1}; it is associated with the compact H II region. The second component has an angular size of $\sim 16''$ and is found projected toward the head of the cometary-like H II region. The average center velocity and width of the carbon line emission are 21.1 ± 0.7 km s^{-1} and 5.1 ± 1.7 km s^{-1}, respectively. The spatial location and velocity of both carbon regions suggest that the emission arises in layers of photodissociated gas at the interface between the molecular cloud and the regions of ionized gas that are undergoing a champagne phase. From a model analysis of the dependence of the recombination line intensity with principal quantum number, we conclude that the carbon emission originates in *warm photodissociated regions.* The electron temperatures and electron densities of the photodissociated gas range between 400 and 600 K and between 40 and 80 cm^{-3}, respectively. Further, we find that stimulated amplification of the background H II region continuum radiation contributes significantly to the carbon emission in both components. We also detected emission in sulfur radio recombination lines from both components. We find that the ratios of sulfur to carbon line intensities are considerable larger than the [S/C] cosmic abundance ratio and that they vary with principal quantum number, with values in the range between 0.3 and 0.6. We attribute the large values of the intensity ratios to depletion of carbon in the gas phase by a factor of ~ 5 and the variations with principal quantum number to stimulated emission effects in a region of low electron density ($n_e \sim 3$ cm^{-3}) and low temperature ($T_e \sim 50$ K) that surrounds the C^+ region.

Subject headings: H II regions — ISM: individual (S88B) — radio lines: ISM

1. INTRODUCTION

Recently formed massive stars are frequently found embedded in the dense cores of molecular clouds, out of which the luminous stars presumably formed (Churchwell, Walmsley, & Cesaroni 1990; Cesaroni et al. 1991; Plume, Jaffe, & Evans 1992). The stellar radiation shortward of the Lyman limit ($\lambda < 912$ Å) ionizes the gas around the recently formed star, creating a compact region of ionized gas. On the other hand, the UV stellar radiation longward of the Lyman limit escapes the H II region and dissociates most molecules and ionizes atoms with ionization potentials less than 13.6 eV around the H II regions, giving rise to regions of partially ionized gas, also called photodissociated regions (PDRs). Since the most abundant of these atoms is carbon, radio recombination lines of carbon are potential probes of the physical conditions and kinematics of the partially ionized gas surrounding H II regions (Gordon 1988; Roelfsema & Goss 1992).

Carbon radio recombination lines arising from C^+ ions in partially ionized transition layers between H II regions and molecular clouds, first detected by Palmer et al. (1967) toward Orion A, have been observed with single-dish instruments toward about a dozen H II regions (Zuckerman & Ball 1974; Pankonin, Thomasson, & Barshun 1977a; Pankonin et al. 1977b; Silverglate & Terzian 1978; Pankonin 1980; Onello, Phillips, & Terzian 1991; Natta, Walmsley, & Tielens 1994; Onello & Phillips 1995). The interpretation of these observations has, however, proved to be difficult (see the reviews by Brown, Lockman, & Knapp 1978; Roelfsema & Goss 1992). The strength of the C^+ line emission depends not only on the physical conditions of the partially ionized medium but also, through the effect of stimulated emission, on the location of the C II region with respect to the H II region. Hence, the determination of the physical properties of PDRs (such as the density and temperature) from observations of C^+ recombination line emission with low angular resolution is not straightforward. A major unresolved question is whether the line emission is dominated by spontaneous transitions (e.g., Hoang-Binh & Walmsley 1974), by stimulated emission caused by the background continuum radiation of the H II region (e.g., Dupree 1974; Silverglate & Terzian 1978), or by a combination of both mechanisms (Pankonin et al. 1977b).

To determine accurately the physical conditions in the PDRs and their relation to the H II regions, measurements of C^+ lines with high angular resolution are needed.

TABLE 1

OBSERVATIONAL PARAMETERS

Date (1)	Configuration (2)	Line (3)	Channels per IF (4)	Width (kHz) (5)	t_{int} (minutes) (6)	Bandpass Calibrator (7)	Θ_{HPBW} (arcsec) (8)	Noise[a] (mJy beam^{-1}) (9)
1995 Mar 28.....	D	C92α	63	48.828	397	0316+413	10.4 × 9.4	0.5
1996 Mar 21.....	C	C166α	127	6.1035	408	0538+498	14.1 × 13.3	1.6
1996 Mar 30.....	C	C110α	127	12.207	437	0316+413	10.2 × 9.1	0.9

[a] 1 σ rms noise in a line channel map.

Accordingly, we have started a long-term project of VLA observations of carbon radio recombination line emission in different frequencies and different configurations, toward several complex regions of ionized gas. The high angular resolution spectroscopic observations should provide the required information, such as the location of the C II region with respect to the H II region, to undertake a detailed modeling of the C^+ emission and hence allow the possibility of determining the physical conditions of the PDR. To date, only a very few C II regions have been observed with high angular resolution (Roelfsema, Goss, & Wilson 1987; Roelfsema & Goss 1991; Onello et al. 1994; Wyrowski et al. 1997). In this paper we report VLA observations of radio recombination lines of carbon toward the S88B region of massive star formation.

The S88B (or G61.48+0.09) H II region complex, located at a distance from the Sun of 5.4 kpc (Churchwell et al. 1990), consists of two regions of ionized gas: an extended ($\sim$14″) cometary-like component, located toward the west (S88B1), and a compact ($\sim$3.″5), brighter component (S88B2), located toward the east (Felli & Harten 1981; Garay et al. 1993). Both regions appear to be undergoing champagne flows (Garay, Lizano, & Gómez 1994, hereafter GLG; Gómez, Garay, & Lizano 1995, hereafter GGL). Radio recombination carbon line emission toward S88B has been detected, with single-dish instruments, in four transitions (C140α and C167α, Silverglate & Terzian 1978; C166α, Silverglate 1984; C168α, Onello et al. 1991). Silverglate & Terzian (1978) explained the observed emission as arising from a partially ionized medium with $30 < T_e < 100$ K and $15 < n_e < 100$ cm^{-3}. However, because of the coarse angular resolution of the single-dish observations, the spatial relationship between the carbon-emitting region and the H II regions could not be established, and hence it was difficult to distinguish whether the carbon line emission corresponds to stimulated emission amplifying the continuum radiation of the H II regions or spontaneous emission. To investigate the nature of the photodissociated region toward S88B in more detail, we made observations of three carbon radio recombination lines with high angular resolution. The main goals of these observations were to determine the physical characteristics of the photodissociated gas, to establish its spatial and kinematical relationship to the regions of ionized gas in S88B, and to determine whether the observed C^+ emission is mainly spontaneous or stimulated emission.

2. OBSERVATIONS

The observations were made with the Very Large Array (VLA) of the National Radio Astronomy Observatory,[1] on 1995 March 28 (C92α line), 1996 March 21 (C166α line), and 1996 March 30 (C110α line). The carbon lines were observed using two intermediate frequencies (IFs) of the four IF spectral line mode of the VLA. The other two IFs were used to simultaneously observe hydrogen recombination lines. The results of the later observations will be described in a separate paper. In each epoch we observed for 10 hours under good weather conditions. Each 20 minute scan on source was paired with a 4 minute calibration scan on 1923+210. The phase center of the array was set at $\alpha(1950) = 19^h44^m43^s.0$ and $\delta(1950) = 25°05'20''.0$.

For the C92α observations we used a bandwidth of 3.125 MHz and 63 spectral channels, each 48.828 kHz wide, which provided a velocity resolution of 1.76 km s^{-1}. The two IFs were centered at the frequency of the He92α line (8312.769 MHz) for an LSR velocity of 22 km s^{-1}. For the C110α observations we used a bandwidth of 1.5625 MHz and 127 spectral channels, each 12.207 kHz wide, which provided a velocity resolution of 0.75 km s^{-1}. The IFs were centered at the frequency of the C110α line (4876.589 MHz) for an LSR velocity of 22 km s^{-1}. For the C166α observations we used a bandwidth of 0.78125 MHz and 127 spectral channels, each 6.1035 kHz wide, which provided a velocity resolution of 1.28 km s^{-1}. The IFs were centered at the frequency of the C166α line (1425.445 MHz) for an LSR velocity of 22 km s^{-1}. The basic observing parameters are summarized in Table 1. Columns (2)–(7) give, respectively, the array configuration, the observed carbon line, the number of channels per IF, the channel separation, the total integration time on source, and the observed calibrator used to normalize the bandpass response.

The data were edited and calibrated by applying the complex gain solution from the calibration source following the standard VLA procedures. The flux density scale was determined by observing the source 3C 286, for which we assumed flux densities of 14.8, 7.5, and 5.3 Jy at 20, 6, and 3.6 cm, respectively. The VLA spectral line system also provides a continuum channel that records the average power of the central 75% of the total available bandpass. This continuum channel was self-calibrated in phase (Schwab 1980), using the Astronomical Image Processing System (AIPS) task CALIB, and the phase corrections were applied to all spectral line channels. To produce maps of line emission, we subtracted an average of all line-free channels from the visibility data of each individual channel, using the task

[1] The National Radio Astronomy Observatory is a facility of the National Science Foundation operated under cooperative agreement by Associated Universities, Inc.

UVLIN. The (u,v) line data were then Fourier transformed and CLEANed using the MX algorithm. Furthermore, in order to produce images with similar angular resolutions at the three observed carbon lines, we also made maps using Gaussian tapers of 20 and 10 kλ for the C110α and C166α line observations, respectively. We note that in these maps the sensitivity to low surface brightness emission was considerably improved. The resulting synthesized half-power beamwidths are given in column (8) of Table 1. The rms noise per beam solid angle in a single spectral line channel map are given in column (9) of Table 1.

3. RESULTS

We detected emission toward the S88B complex in all three observed carbon radio recombination lines. Maps of the C92α, C110α, and C166α average line emission are shown in Figure 1 (crosses mark the position of the peak radio continuum emission from the B1 and B2 H II regions). We find that the C^+ line emission arises from a region with a size of $\sim 34'' \times 18''$, which is closely associated with the H II regions. The quoted size corresponds to the geometric average of the individual sizes observed in each of the three transitions. The peak of the C^+ emission lies near the peak of the most compact H II region. We have separated the C^+ emission as arising from two distinct components: a compact component with a deconvolved FWHM angular size of $\sim 6''.6$, associated with the compact H II region S88B2 [hereafter the S88B:(C^+)east component], and a more extended component with a deconvolved FWHM angular size of $\sim 16''$, associated with the head of the more extended cometary-like H II region S88B1 [hereafter the S88B:(C^+)west component]. The boxes shown in the upper panel of Figure 1 indicate the areas on the sky over which we integrated to obtain the spectra of the (C^+)east and (C^+)west components.

The spectra of the spatially integrated emission from the east and west components, in the LSR velocity range from -5 to 40 km s^{-1}, are displayed in Figure 2. Two features are present in all but one of these spectra. The stronger feature, at the velocity of ~ 21 km s^{-1}, corresponds to the emission from the carbon recombination line. The weaker feature, at the velocity of ~ 12.5 km s^{-1}, corresponds to emission from a recombination line of an element heavier than carbon. The difference in velocity between this line and the carbon line, ~ 8.5 km s^{-1}, suggests that the emission can be attributed to sulfur, as already concluded by Silverglate (1984) and Onello et al. (1991). Hereafter we will assume that this line corresponds to sulfur emission but note that, because of its relatively broad line width, it is possible that some power may be due to emission from silicon. The parameters of the C^+ and S^+ integrated line emission from each component, determined by fitting two Gaussians to the observed spectra, are given in Table 2. The fitted Gaussian profiles are shown in Figure 2 as continuous lines.

The average line-center velocities of the carbon emission from the (C^+)east and (C^+)west components are 21.0 ± 0.5 and 21.1 ± 0.7 km s^{-1}, respectively. The line widths are typically ~ 5 km s^{-1}. Given its narrow line width and strength, it is highly improbable that the C^+ emission originates from within the H II regions. If the C^+ gas were inside the H II region, it would share the same turbulent velocity dispersion as the H^+ gas. The observed widths of the hydrogen recombination line emission from the H II regions, ~ 26

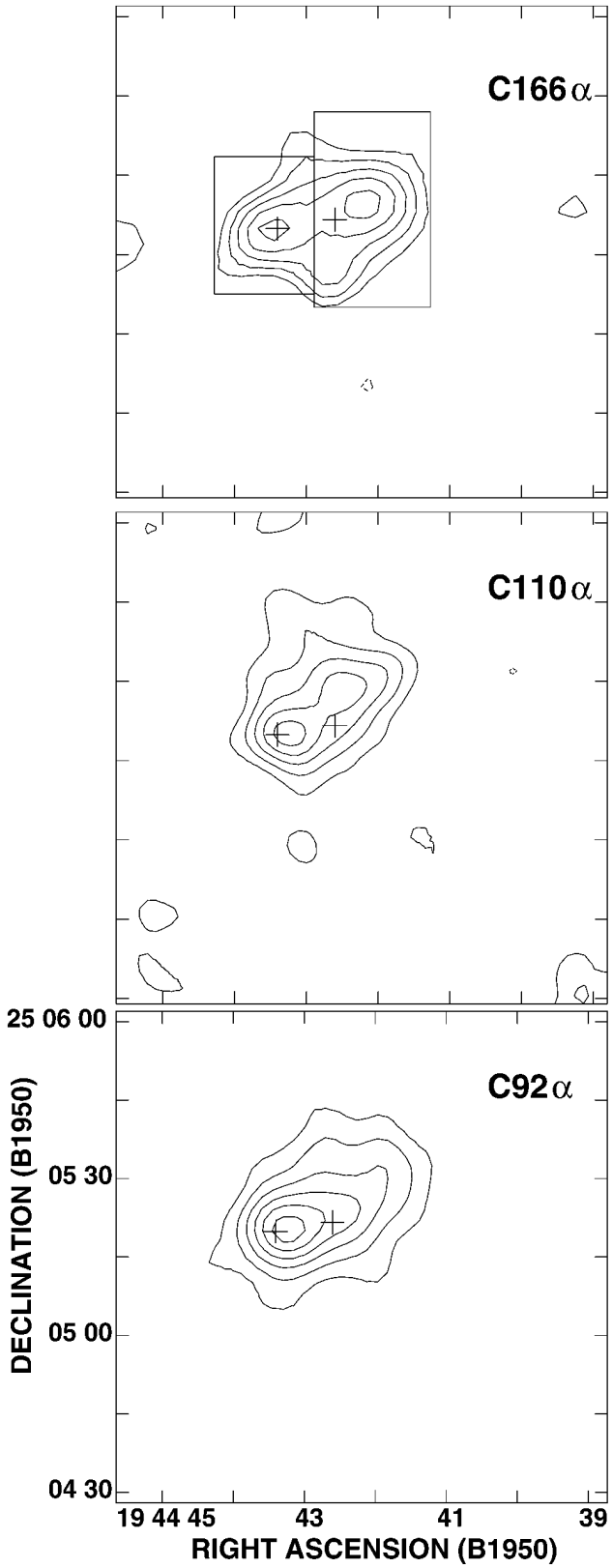

FIG. 1.—VLA maps of the ionized carbon emission from S88B. The crosses mark the peak position of the S88B1 (*right*) and S88B2 (*left*) H II regions. *Upper panel*: C166α average line emission. Contour levels are (-2, 2, 3, 4, 5, 6) $\times$ 1.5 mJy beam^{-1}. The angular resolution (FWHM beam) is $14''.1 \times 13''.3$. The boxes indicate the areas on the sky over which we integrate to obtain the spectra of the (C^+)east and (C^+)west components. *Middle panel*: C110α average line emission. Contour levels are (-1, 1, 2, 3, 4, 5) $\times$ 1.4 mJy beam^{-1}. The angular resolution is $10''.2 \times 9''.1$. *Lower panel*: C92α average line emission. Contour levels are (-2, 2, 3, 4, 5, 6) $\times$ 1.0 mJy beam^{-1}. The angular resolution is $10''.4 \times 9''.4$.

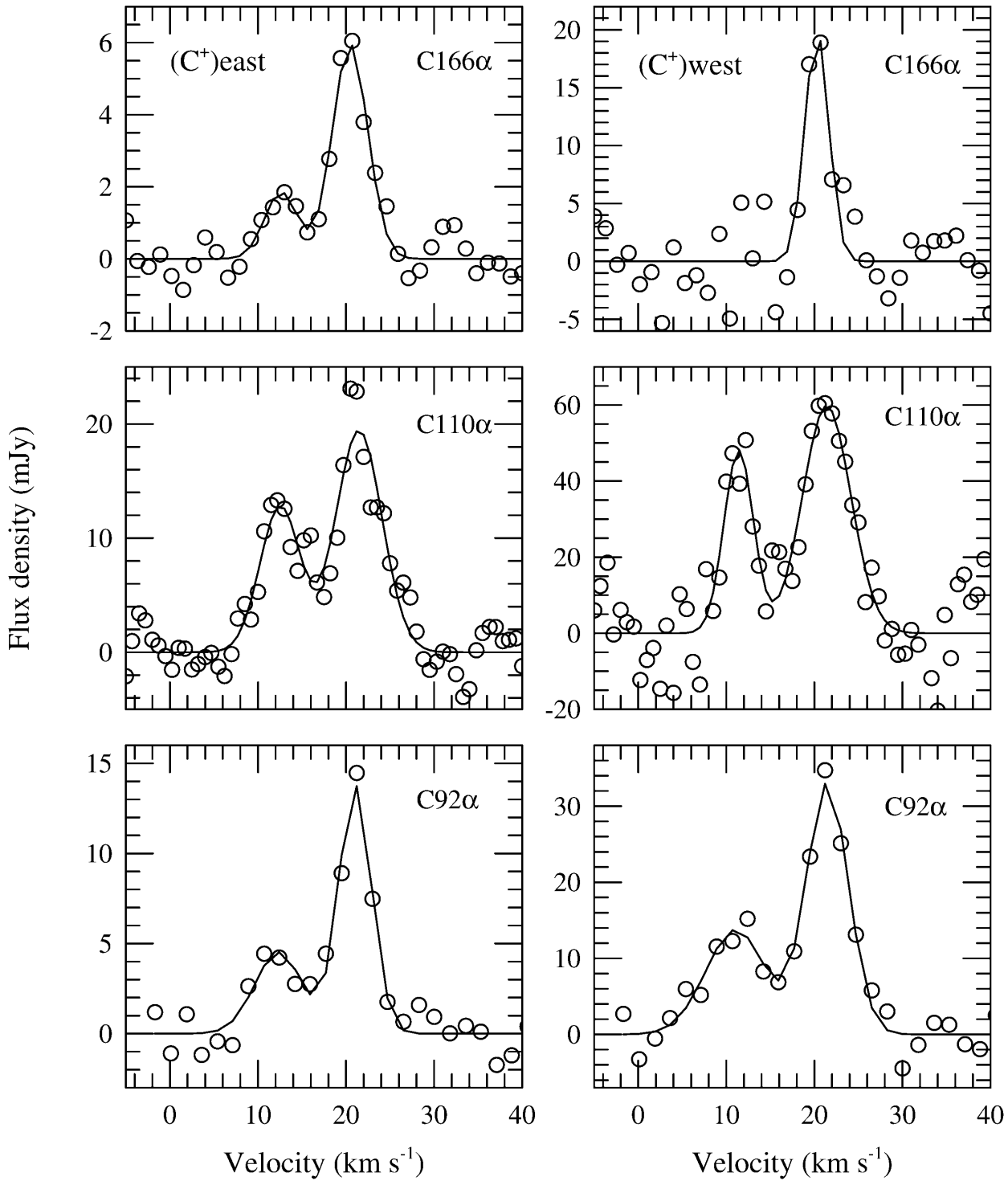

FIG. 2.—Spectra of the spatially integrated carbon line emission from the (C^+)east (*left*) and (C^+)west (*right*) sources. *Upper panel*: C166α spectrum. *Middle panel*: C110α spectrum. *Lower panel*: C92α spectrum. The feature at the velocity of ~ 21 km s^{-1} corresponds to the emission from the carbon recombination line. The weaker feature, at the velocity of ~ 12.5 km s^{-1}, corresponds to emission from the sulfur recombination line. The continuous lines show the result of fits to the observed data (*open circles*).

km s^{-1}, and electron temperatures of the gas, $\sim 10^4$ K (GLG), imply a turbulent broadening of ~ 15 km s^{-1}, considerably larger than the width of the carbon lines. The C^+ emission most likely originates in a photodissociated region separating the H II regions from the molecular cloud (see § 4). From single-dish observations, with a beam of 3.′2, Silverglate (1984) measured a line strength in the C166α line of 29 mJy, in good agreement with the value measured by us with 20-fold higher spatial resolution, 27 ± 3 mJy. This result indicates that there is negligible C^+ emission from an hypothetical extended component, which would have been resolved out by the VLA.

Individual line channel maps from the C110α observations, in the velocity range 7.0–28.8 km s^{-1}, are shown in Figure 3. The channel width is 0.75 km s^{-1}. The emission detected in the range of velocities from 19.0 to 24.3 km s^{-1}

TABLE 2

OBSERVED LINE PARAMETERS

Line	S_L (mJy)	V (km s^{-1})	Δv (km s^{-1})	$\int S_L dv$ (mJy km s^{-1})
S88B:(C$^+$)east				
C166α.....	6.0 ± 0.4	20.5 ± 0.1	4.7 ± 0.3	28.0 ± 1.9
S166α	1.9 ± 0.4	21.1 ± 0.4	4.4 ± 1.0	8.2 ± 1.8
C110α.....	19.5 ± 1.1	21.5 ± 0.2	6.2 ± 0.5	120.0 ± 8
S110α	12.8 ± 1.1	21.0 ± 0.3	5.4 ± 0.6	69.0 ± 8
C92α	13.8 ± 0.9	21.0 ± 0.1	4.4 ± 0.3	60.2 ± 4.4
S92α	4.5 ± 0.7	20.8 ± 0.5	6.3 ± 1.5	28.7 ± 6.4
S88B:(C$^+$)west				
C166α.....	19.9 ± 2.5	20.3 ± 0.2	3.2 ± 0.5	63.1 ± 8.7
C110α.....	59.8 ± 4.6	21.4 ± 0.2	6.5 ± 0.6	387.0 ± 36
S110α	48.1 ± 5.8	19.9 ± 0.2	3.9 ± 0.6	189.0 ± 26
C92α	33.0 ± 1.7	21.5 ± 0.1	5.6 ± 0.4	185.0 ± 12
S92α	13.8 ± 1.5	19.6 ± 0.4	8.0 ± 1.2	110.0 ± 18

corresponds to the emission in the C110α line, while the emission detected in the range of velocities from 10.0 to 13.0 km s^{-1} corresponds to emission from the S110α line. This figure shows that the angular extent of the C110α and S110α emitting regions are roughly similar. From a fit to the spatial distribution of the velocity-integrated line emission, with a single Gaussian component, we find a FWHM deconvolved size of 27″ × 18″, P.A. 139°, for the C110α emission and a FWHM deconvolved size of 24″ × 19″, P.A. 122°, for the S110α emission.

4. DISCUSSION

4.1. C$^+$ *Line Intensities*

The strength of the C$^+$ recombination line emission is a function not only of the physical conditions in the photodissociated medium but also of the location of the C II region along the line of sight. If the C II region is behind or beside the H II region, the line emission is likely to be spontaneous emission. If the C II is in front of the H II region, the line emission will be a superposition of spontaneous emission and emission stimulated by the continuum radiation from the H II region. In general, the line brightness temperature, T_L, of a carbon recombination line from an isothermal, homogeneous, partially ionized medium is given by (see Hoang-Binh & Walmsley 1974)

$$T_L = T_e\left(\frac{b_m\tau_L^* + \tau_C}{b_n\tau_L^*\beta + \tau_C}\right)[1 - e^{-(\tau_L+\tau_C)}] - T_e \times (1 - e^{-\tau_C}) - T_o e^{-\tau_C}(1 - e^{-\tau_L}) , \quad (1)$$

where τ_L, τ_L^*, and τ_C are the line optical depth, the line optical depth under LTE conditions, and the continuum optical depth, respectively. The value T_e is the electron temperature of the partially ionized region; T_o is the main-beam brightness temperature of a background continuum source; n and m are the principal quantum numbers of the lower and upper levels of the transition, respectively; and b and β are the usual departure coefficients from LTE (Dupree & Goldberg 1970). The LTE line optical depth for a C$n\alpha$ line, τ_L^*, is given by

$$\tau_L^* = 5.75 \times 10^2\left(1 + \frac{1.5}{n}\right)\frac{n_e n(\mathrm{C}^+)L}{T_e^{2.5}\Delta v\, \nu}\, e^{157800/n^2T_e} , \quad (2)$$

where n_e and $n(\mathrm{C}^+)$ are, respectively, the electron and ionized carbon densities in cm^{-3}, Δv is the FWHM line width in km s^{-1}, ν is the frequency of the line in GHz, and L is the path length in pc. The continuum optical depth is given by

$$\tau_C = 0.0823\,\frac{n_e n_i L}{T_e^{1.35}\nu^{2.1}} , \quad (3)$$

where n_i is the total density of ions in the C II region in cm^{-3}. Equations (1)–(3) show that the line brightness is a function—through τ_C, τ_L^*, b, and β—of the electron temperature, electron density, carbon ion density, and path length of the C II region and of the brightness of the background source. Thus, in general, a range of values of the physical parameters can reproduce the observed brightness of a single recombination line. Observations of three carbon lines would, on the other hand, provide constraints on the physical parameters of the C II region, allowing a determination of the electron temperatures, densities, and sizes of the carbon region and an investigation of whether the line emission is mainly spontaneous or stimulated.

In order to derive the physical parameters of the C$^+$ region, we computed the intensity of carbon radio recombination lines as a function of principal quantum number for homogeneous, isothermal models. We assume that the total hydrogen number density of the PDR, n_{H}, is given by the condition of pressure equilibrium between the PDR and its associated H II region. The derived n_{H} densities are $\sim 4 \times 10^5$ cm^{-3} and $\sim 2 \times 10^5$ cm^{-3} for the (C$^+$)east and (C$^+$)west regions, respectively (see discussion below). Assuming (1) ionization of all carbon within the PDR, (2) a carbon-to-hydrogen cosmic abundance ratio of 3.7×10^{-4} (Cameron 1973), and (3) a depletion factor, f, of 5—required to explain the observed sulfur-to-carbon line ratios (see discussion below)—then the number density of C ions, $n(\mathrm{C}^+) = n_{\mathrm{H}}[\mathrm{C/H}]/f$, is $7.4 \times 10^{-5} n_{\mathrm{H}}$ cm^{-3}. The free parameters in our model are the electron temperature, the electron density, and the path length of the PDR. The brightness temperature of the background source, another free parameter of the model, is in our case constrained from the observations of the radio continuum emission. The departure coefficients were calculated using the Brocklehurst & Salem (1977) general program for computation of the b_n factors.

Models were computed for a range of electron densities between 10 and 100 cm^{-3} and electron temperatures between 10 and 1000 K. The goal was to relate the observed intensities in the three carbon recombination lines to the physical parameters of the photodissociated gas. In Figure 4 we plot the line brightness temperature of the carbon emission as a function of principal quantum number for both C$^+$ components. The line brightness temperatures, derived from the observed peak line flux densities in a ∼10″ beam assuming unity beam filling factors, are $T_L(\mathrm{C92}\alpha) =$ 1.1 K, $T_L(\mathrm{C110}\alpha) = 4.6$ K, and $T_L(\mathrm{C166}\alpha) = 48$ K for (C$^+$)east and $T_L(\mathrm{C92}\alpha) = 0.75$ K, $T_L(\mathrm{C110}\alpha) = 4.0$ K, and $T_L(\mathrm{C166}\alpha) = 59$ K for (C$^+$)west. The results of the model that best fit the observed trend are shown as continuous lines. We assumed that the main-beam brightness temperature of the background continuum source depends with frequency as $T_o = A(\nu/8.3\ \mathrm{GHz})^{-2.1}$, as is expected for an H II region. For the continuum background sources toward the (C$^+$)east and (C$^+$)west components, we used $A = 80$

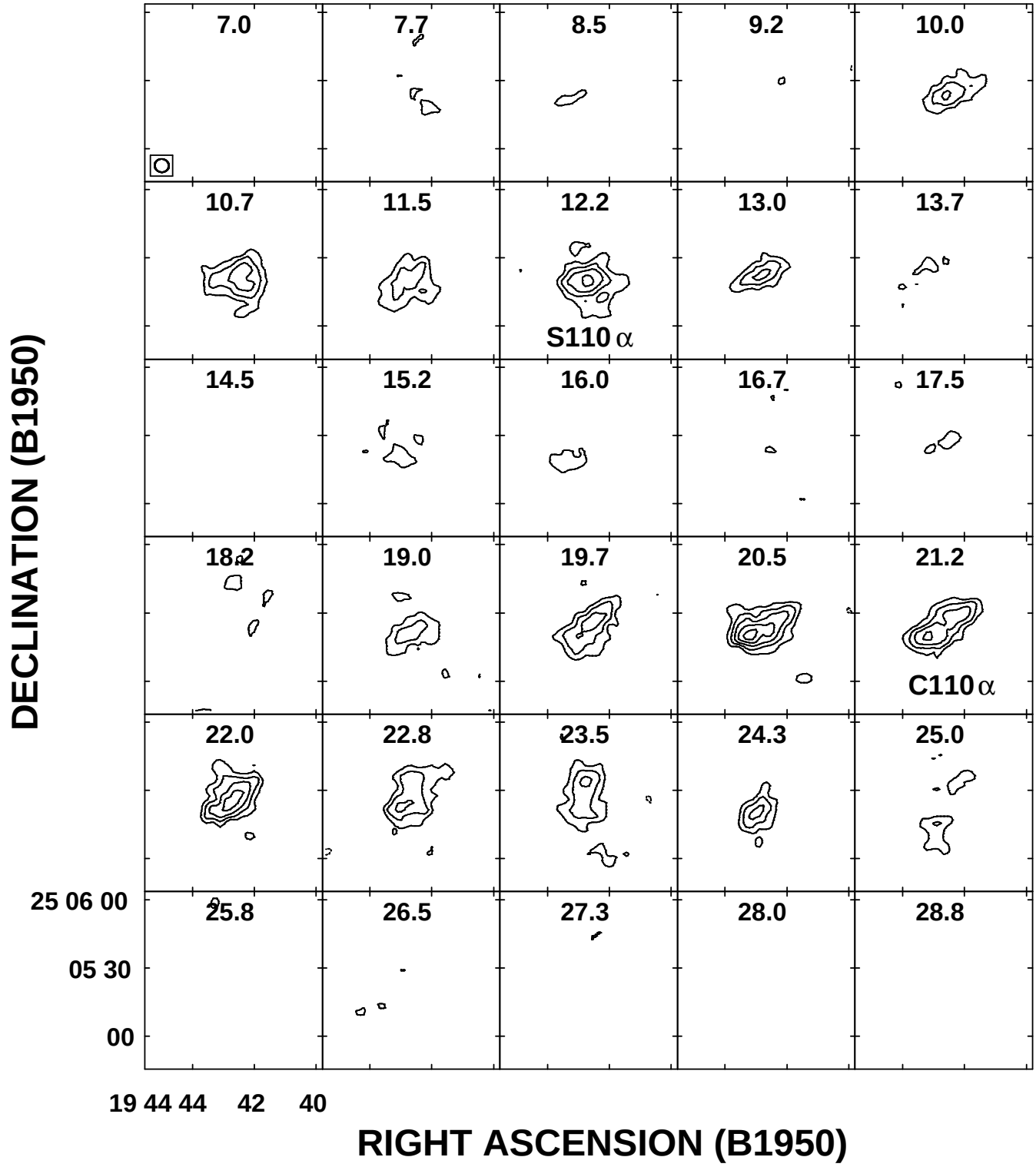

FIG. 3.—Channel maps of the line emission from the C110α observations toward S88B. The LSR velocity, in km s^{-1}, is indicated in the top of each line map. Contour levels are $(-2, 2, 3, 4, 5, 6) \times$ 1.5 mJy $beam^{-1}$. The emission detected in the range of velocities from 19.0 to 24.3 km s^{-1} corresponds to emission in the C110α line, while the emission detected in the range of velocities from 10.0 to 13.0 km s^{-1} corresponds to emission in the S110α line. The angular resolution is 10″.2 × 9″.1.

and 60 K, respectively. These values were derived from the radio continuum observations with a 10″ beam. We find that the observed brightness of the carbon emission from the (C^+)east and (C^+)west components is best matched with models in which the photodissociated gas has electron temperatures of ~600 and ~400 K and electron densities of ~80 and ~40 cm^{-3}, respectively. The derived parameters (T_e, n_e, L) of the C II regions are summarized in Table 3. In addition, we find that amplification of the radio continuum radiation from the background H II region contributes significantly to the C^+ emission, particularly at the higher principal quantum number. To illustrate this point we also

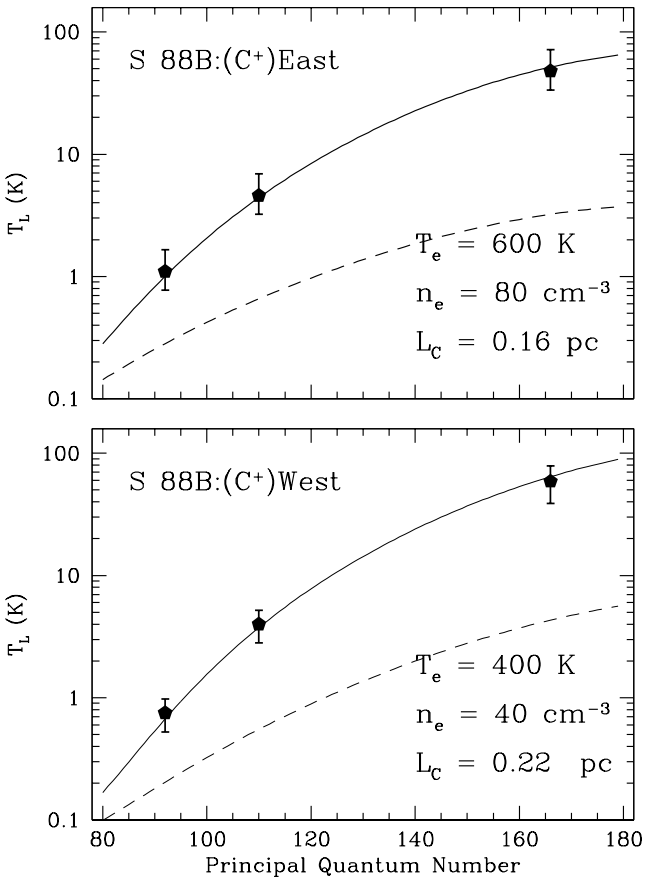

FIG. 4.—Brightness temperature of carbon recombination line emission as a function of principal quantum number. The continuous line indicates the best fit to the observed trends (*pentagons*) assuming a simple model of a homogeneous, isothermal, photodissociated region, as described in the text. The derived parameters are given in the lower right corner of each panel. The broken line indicates the results of the model with the same physical parameters but with no background continuum source. *Upper panel*: S88 B:(C^+)east component. *Lower panel*: S88B:(C^+)west component.

show in Figure 4 the results of a model of the line brightness from a photodissociated region with the physical parameters given in Table 3 but with no background continuum source (*broken line*).

Further, to assess the extent to which the line intensities are affected by the thermal radiation field from the immediately adjacent H II region—through the additional transition rates in the statistical equilibrium equations—we computed models incorporating the presence of an incident radiation field from an H II region with a temperature of 10,000 K and an emission measure of 9×10^6 pc cm^{-6}. We find that, at the electron temperature and electron densities of the PDR, such effect on the line intensities is negligible. As mentioned above, the parameters given in Table 3 were derived assuming values of n_H estimated from pressure equilibrium arguments. Even though this assumption seems reasonable, we still investigated how variations in the value of the neutral hydrogen density (by a factor of 3) affect the derived parameters of the photodissociated region. The main effect of decreasing n_H by a factor of 3 is to produce a decrease in the electron temperature by a factor of ~ 2, while an increase in n_H by a factor of 3 is mainly reflected in a decrease of the path length by roughly a factor of 3. We nevertheless stress that the most relevant conclusion from our modeling, that the PDRs are warm, remains unalterable. It is worthwhile mentioning that the isothermal slab models discussed here require neutral hydrogen column densities of $\sim 2 \times 10^{23}$ cm^{-2} in order to reproduce the observed carbon radio recombination line intensities. Detailed models of PDRs that include the chemistry and heat balance in these regions have been studied by several authors (e.g., Tielens & Hollenbach 1985; Sternberg & Dalgarno 1989; Burton, Hollenbach, & Tielens 1990; Draine & Bertoldi 1996; Störzer, Stutski, & Sternberg 1996; Spaans & van Dishoeck 1997). In particular, in the models studied by Tielens & Hollenbach (1985), the ionized carbon region has $N_H \sim$ a few times 10^{22} cm^{-2}, almost independent of the density of the PDR and the strength of the incident far-ultraviolet (FUV) field. On the other hand, the large column densities we find (as well as the high temperatures) are similar to those derived by Natta et al. (1994), Luhman et al. (1997), and Wyrowski et al. (1997) for PDRs in Orion. In the calculations of the b and β departure coefficients, we did not consider the influence of dielectronic recombination in the level population of carbon atoms (Walmsley & Watson 1982). While no computations of the dielectronic departure coefficients have been reported for the conditions of the photodissociated regions under study, an extrapolation of the Walmsley & Watson (1982) results predicts that the differences between hydrogenic and dielectronic b coefficients should be smaller than 15% for principal quantum numbers in the range 90–170. These differences will modify neither our conclusion regarding the values of the physical parameters nor the conclusion reached concerning the importance of stimulated emission. The good fit to the observations made using hydrogenic departure coefficients suggests in fact that dielectronic recombination is not an important process under the conditions of the regions investigated here. Finally, photodissociated regions are unlikely to be isothermal or homogeneous (Tielens & Hollenbach 1985); thus the physical parameters derived from our models should be taken only as representative of the conditions of the bulk of the emitting region.

TABLE 3

DERIVED PARAMETERS OF C^+ REGIONS

Component	T_e (K)	n_e (cm^{-3})	L (pc)	n_H (cm^{-3})
S88B:(C^+)east	600	80	0.16	4×10^5
S88B:(C^+)west.....	400	40	0.22	2×10^5

4.2. S^+ *Line Intensities*

Sulfur radio recombination lines have been detected, with single-dish instruments, toward a number of regions of star formation where carbon recombination lines have been detected (see Chaisson et al. 1972; Pankonin et al. 1977b). In particular, the detection of emission in a sulfur radio recombination line toward the S88B complex was first reported by Silverglate (1984), who found that the ratio of integrated 166α line intensities of sulfur and carbon is 0.39 ± 0.06, about 9 times larger than the cosmic abundance ratio of 0.042 (Cameron 1973). Onello et al. (1991) reported a S168α/C168α intensity ratio of 0.31. The most likely explanation for the discrepancy between the observed intensity ratios and the cosmic abundance ratio is that a large fraction of carbon is depleted onto dust grains

(Knapp, Kuiper, & Brown 1976). Sulfur is known to be relatively undepleted in the interstellar medium (Morton 1974; Sofia, Cardelli, & Savage 1994).

We find that the sulfur-to-carbon ratios of line intensities show significant variations with principal quantum number. In Table 4 we give the integrated S/C intensity ratios observed toward both the (C^+)east and (C^+)west regions. The S166α/C166α ratios, of $\sim$0.3, are smaller, roughly by factors of 1.5–2, than the S92α/C92α and S110α/C110α ratios. This result suggests not only that the ratios of intensities reflect the ratio of abundances in the gas phase, but also that stimulated effects play an important role in the observed variations.

In order to assess quantitatively the importance of stimulated effects in the line ratios, we have computed intensities of carbon and sulfur lines using a simple model of the line transfer equation under non-LTE conditions in a two-zone medium. In the first zone (the C^+ region) both carbon and sulfur are ionized, while in the second zone (hereafter the S^+ region), which has a lower electron density and temperature than the first one, only sulfur is ionized. In our calculations we assume that the b and β departure coefficients have the same values for all hydrogenic atoms. We find that stimulated emission effects within the C^+ region itself are almost identical for the carbon and sulfur lines and, therefore, that they do not produce significant differences in the line intensity ratios with principal quantum numbers. We conclude that the presence of a medium with lower density and lower temperature than the C^+ region—and in front of it—is required to explain the variations in the intensity ratio with principal quantum number. In a PDR these conditions are naturally found beyond the C^+ region, since the softer photons that escape the C^+ region can still ionize sulfur, which has a ionization potential lower than that of carbon and a factor of $\sim$24 lower cosmic abundance. Therefore, the size of the S^+ region is expected to be larger, the mean electron density lower, and the temperature colder than that of the C^+ region. We can roughly reproduce the observed ratios if the depletion factor of carbon is $\sim$5 and if the S^+ region has an electron temperature of 50 K, an electron density of $\sim$3 cm^{-3}, and a path length of 0.34 pc. Even though there may be a range of physical parameters of the S^+ region that could explain the observations, the quoted solution seems the most reasonable. Finally, we note that the observations show that the C^+ and S^+ regions have similar angular sizes, while here we require that the S^+ region be larger. These two results are not in contradiction, however, since the observed emission from the C^+ and S^+ regions is mainly stimulated emission, and hence the observed angular sizes reflect the angular size of the background H II region, not the actual size of the regions.

TABLE 4

S/C Intensity Ratios

Component	Line	$\frac{(\int T_L\,dv)_S}{(\int T_L\,dv)_C}$
S88B:(C^+)east	166α	0.29 ± 0.07
	110α	0.58 ± 0.08
	92α	0.48 ± 0.11
S88B:(C^+)west.....	166α	...
	110α	0.49 ± 0.08
	92α	0.59 ± 0.10

4.3. *The Relationship between the Photodissociated, Ionized, and Molecular Gas*

The knowledge of the spatial distribution and velocity field of the observed H II, C^+, and NH_3 emission from the S88B complex allows us to examine the physical and kinematical relationship between the ionized, photodissociated, and molecular gas toward this region. Figure 5 presents a summary of the spatial distribution of emission in the different physical components. The upper panel shows a map of the average C166α line emission superposed on a contour map of the 1.4 GHz radio continuum emission, as observed with the same synthesized beam as the carbon observations (14.″1 × 13.″3). The middle and lower panels show contour maps of the velocity-integrated ammonia emission in the (3, 3) line as seen with the VLA (taken from GGL) superposed, respectively, on a contour map of the 8.3 GHz radio continuum emission as observed with a 2.″4 × 2.″1 beam (taken from GLG) and on a contour map of the average C92α line emission. Figure 5 clearly shows that there is a close spatial correspondence between the C^+ components, NH_3 clumps, and the regions of ionized gas, which brings up the question of their physical association. In what follows, we discuss the physical relationship between the ionized, partially ionized, and warm molecular components.

4.3.1. *S88B*: (C^+) *East Component*

The S88B:(C^+)east component is spatially coincident with the S88B2 H II region and with the bright ammonia clump S88B:(NH_3)east. GGL found that the ammonia emission from this clump arises from a warm gas with a temperature of either 70 or 140 K, depending on whether the clump is, respectively, behind or in front of the H II region. The ammonia clump has a size of $\sim$0.07 pc, an average molecular hydrogen density of 3×10^4 cm^{-3}, and an average line-center velocity of 21.9 ± 0.2 km s^{-1}. On the other hand, GLG found that the region of ionized gas has a diameter of $\sim$0.1 pc, an average electron density of 1.5×10^4 cm^{-3}, an average line-center velocity of 18.1 ± 0.5 km s^{-1}, and a FWHM line width of 26.9 ± 1.4 km s^{-1}. We find that the C^+ emission from the east component arises from a photodissociated region with an electron density of $\sim$ 80 cm^{-3} and an electron temperature of $\sim$600 K. This value of the electron temperature, implying a thermal width of 1.5 km s^{-1}, suggests that the observed width of the carbon emission, of $\sim$5 km s^{-1}, is mainly produced by a turbulent component with a velocity dispersion, $\sigma_{\rm turb}$, of $\sim$2.0 km s^{-1}. Since the turbulent velocity dispersion is shared by both the C and H gas, the velocity dispersion of the hydrogen gas in the PDR is $\sigma_{\rm H} = (\sigma^2_{\rm turb} + \sigma^2_{\rm Hth})^{1/2} = 3.0$ km s^{-1}. Assuming pressure equilibrium between the H II region and the PDR, $n_{\rm H} = 2n_e(\sigma_{\rm H\,II}/\sigma_{\rm H})^2 \sim 4 \times 10^5$ cm^{-3}, which was the hydrogen number density assumed in our modeling. An alternative estimate of the gas density can be made from the observations of the sulfur emission. Assuming that sulfur is fully ionized and that the [S/H] abundance ratio in the gas phase is 1.6×10^{-5} (equal to the cosmic abundance ratio), we derive that the density of neutral hydrogen is $n_{\rm H} \sim 2 \times 10^5$ cm^{-3}, in good agreement with the previous estimate.

From the derived electron density of 80 cm^{-3} and hydrogen density of $\sim 4 \times 10^5$ cm^{-3}, we find that the ionization fraction, $x = n_e/n_{\rm H}$, within the PDR is $\sim 2 \times 10^{-4}$. The ionization fraction that is expected if all the electrons come from the ionization of carbon in the gaseous phase is

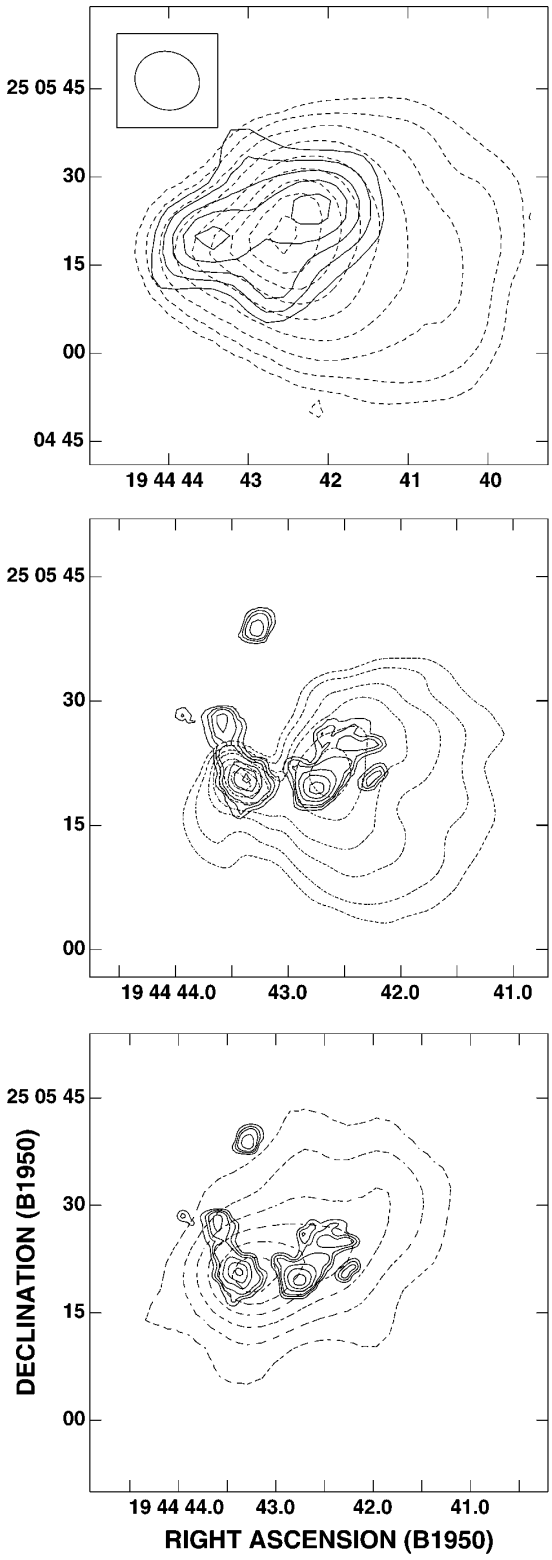

FIG. 5.—*Upper panel*: Contour map of the average C166α line emission (*continuous line*) superposed on a contour map of the 1.4 GHz radio continuum emission (*broken line*). Contour levels are 2.5, 5, 10, 20, 35, 50, 65, 80, and 95 percent of the peak flux density of 0.86 Jy beam^{-1} for the continuum emission, and the same as in Fig. 1 for the line emission. The angular resolution is 14.″1 × 13.″3. *Middle panel*: Contour map of the velocity-integrated ammonia emission (*continuous line*; taken from GGL) superposed on a contour map of the 8.3 GHz radio continuum emission (*broken line*; taken from GLG). *Lower panel*: Same ammonia map as in middle panel superposed on a contour map of the C92α average line emission (*broken line*). Contour levels are the same as in Fig. 1.

$x = [C/H]/f$, where f is the carbon depletion factor. Using $f = 5$, we find that $x = 7.4 \times 10^{-5}$, about 3 times smaller than the one derived from the modeling, implying that another source of electrons is needed. Taking the ionization of other metals, such as Si, S, and Mg, into account as a source of electrons, we still find a shortage of electrons by a factor of ~ 1.5. It is possible that some of the electrons in the PDR might come from ionizations of hydrogen. This suggestion is strongly supported by the observations of Garay et al. (1998), who detected emission from narrow hydrogen radio recombination lines arising from a partially ionized gas with an electron temperature of ~ 800 K toward this region.

The line-center velocities of the different tracers give us a clue as to whether the PDR is in pressure equilibrium with its surroundings. The average line-center radial velocity of the C^+ emission, 21.2 km s^{-1}, is similar to the radial velocity of the large-scale ambient molecular cloud, ~ 22.0 km s^{-1}, as determined from observations with low angular resolution (HPBW of 40″; Macdonald et al. 1981; Churchwell et al. 1990). The small difference in velocities suggests that the PDR is in quasi–pressure equilibrium, slowly expanding into the quiescent ambient molecular cloud. The average line-center velocity of the B2 H II region, 18 km s^{-1}, is consistent with the ionized gas undergoing a champagne flow in a direction that is inclined *toward the observer*, in which case the mean velocity of the ionized gas is expected to appear blueshifted. In fact, Figure 14 of GGL shows that the velocity of the ionized gas at the head of the champagne flow is ~ 21 km s^{-1}, indicating that the PDR is in quasi-equilibrium with the H II region, as assumed in our modeling. Finally, we note that the velocity of the ammonia emission from the (NH_3)east clump is almost identical to that of the ambient cloud. The heating of the NH_3 clump is thus probably provided by the radiation from the exciting star. In conclusion, the similar line-center velocities of the different gas components at the head of the B2 region indicate that they are in a quasi-equilibrium.

4.3.2. *S88B*:(C^+) *West Component*

The S88B:(C^+)west component is associated with the S88B1 cometary H II region (GLG) and with the S88B:(NH_3)west ammonia clump (GGL). GLG found that the velocity of the ionized gas from the B1 H II region increases from ~ 21 km s^{-1} at the head position to ~ 33 km s^{-1} in the tail's region, and they suggested that this cometary H II region is undergoing a champagne flow. In addition, they found that the ionized gas has an average electron density of 3.2×10^3 cm^{-3}, an average line-center velocity of 28.4 ± 0.2 km s^{-1}, and a line width of 25.6 ± 0.5 km s^{-1}. The S88B:(NH_3)west clump is located close to the head of the cometary H II region, has a size of ~ 0.08 pc, and a mean line-center velocity of ~ 21.6 km s^{-1}, similar to the ambient molecular cloud velocity. Assuming that the (NH_3)west ammonia clump is in front of the H II region, GGL derived that the emission arises from warm gas with a temperature of ~ 80 K, a total ammonia column density of $\sim 1 \times 10^{16}$ cm^{-2}, and a molecular hydrogen density of 4×10^4 cm^{-3}.

We find that the C^+ emission from the west component arises from a photodissociated region with an electron density of ~ 40 cm^{-3} and an electron temperature of ~ 400 K. The assumption of pressure equilibrium gives, in this case, $n_H \sim 2 \times 10^5$cm^{-3}. As in the case of (C^+)east, the line-center velocities of the C^+, H II, and NH_3 regions in S88B1

indicate that the PDR, at the head of the cometary H II region, is in quasi–pressure equilibrium with its surroundings. The implied ionization fraction in the PDR is $\sim 2 \times 10^{-4}$. Garay et al. (1998) did not detect emission from a partially ionized hydrogen gas toward this H II region.

The carbon emission does not cover the full angular extent of the S88B1 region but is roughly projected toward the head structure of this cometary H II region. The observed spatial distribution of C^+ can be explained as produced by the illumination, by the FUV radiation from the central hot star, of the surrounding nonuniform molecular cloud. There are two effects that produce observable C^+ emission only toward the head of the cometary H II region. First, as discussed above, this emission is due mainly to the stimulated amplification of the background continuum radiation field from the H II region. This continuum is strongest at the head of the cometary, since the gas becomes more optically thin toward the tail. A second effect is due to the density gradient of the cloud. Theoretically, the intensity of radio recombination lines is expected to decrease with decreasing electron density. Thus, in regions with large density gradients, the intensity of the carbon line emission along the lines of sight in which the ambient medium density is low should be considerably weaker than the emission-line intensity toward the high electron density regions. In fact, single-dish observations of molecular line emission toward the S88B H II complex suggest that the density of molecular gas falls off, roughly in a east-west direction, away from the S88B1 H II region (Evans et al. 1981; White & Fridlund 1992). The presence of such density gradients is also supported by the results of the recombination line observations of the ionized gas of GLG, which implies that the density decreases with distance west of the leading edge of the cometary region.

We suggest that the (C^+)west region corresponds to a photodissociated region adjacent to a blister H II region, delineating the photodissociated wall of the cavity formed by the evacuation of the ionized gas toward the region of lower density. The lack of extended C^+ emission can then be understood as reflecting the decrease in the background continuum and in the C^+ density with increasing distance west of the focus of the cometary region. The column densities of C^+ toward the tail of the cometary region are probably insufficient to produce detectable emission in the radio recombination lines. Additional support for the blister-PDR hypothesis is provided by the similar velocities of the C^+ emission, 21.1 ± 0.7 km s^{-1}, and of the ionized gas at the head position, ~ 21 km s^{-1}. Finally, the similar velocities of the (NH_3)west ammonia clump and ambient molecular gas suggest that this clump is part of the denser ambient gas that is heated, and thus illuminated, by the FUV radiation from the luminous exciting star of the S88B1 H II region.

5. SUMMARY

With the VLA, we observed the C92α, C110α, and C166α radio recombination lines of carbon from the S88B massive star forming region. The main results and conclusions presented in this paper are summarized as follows.

The line images show that the spatial distribution of the emission in the three carbon lines is very similar, arising from a region with an overall angular size of $\sim 34'' \times 18''$. The C^+ emission can be decomposed into two distinct components: (*a*) an eastern component, S88B:(C^+)east, having an angular size of $\sim 6''.6$, an average line-center velocity of 21.0 ± 0.5 km s^{-1}, and an average line width of 5.1 ± 1.0 km s^{-1}; and (*b*) a western component, S88B:(C^+)west, having an angular size of $\sim 16''$, an average line-center velocity of 21.1 ± 0.7 km s^{-1}, and a line width of 5.1 ± 1.7 km s^{-1}.

We find that the carbon components are closely associated with the regions of ionized gas and with warm and dense ammonia clumps within the S88B complex. The (C^+)east carbon component is intimately associated with the S88B2 compact H II region (Felli & Harten 1981) and with the (NH_3)east ammonia clump (Gómez et al. 1995). The observed spatial distribution and relative velocities strongly suggest a physical association between the different gas components, with the carbon emission originating in a photodissociated region that separates the region of ionized gas from the warm and dense ammonia clump. The (C^+)west carbon component is found projected close to the head of the S88B1 cometary-like H II region. The spatial location and velocity of the (C^+)west region suggest that the carbon emission arises in a layer of photodissociated gas at the interface between a nonuniform-density molecular cloud and a region of ionized gas that is undergoing the champagne phase.

We analyzed the observed dependence of the carbon line intensity on principal quantum number, using a simple model of the brightness of the line radiation from a homogeneous, isothermal, photodissociated region. Our modeling strongly indicates that the carbon emission from the S88B region originates in *warm photodissociated regions.*

From the best fit to the observed trends, we derive the result that the photodissociated regions have electron temperatures in the range between 400 and 600 K and electron densities in the range between 40 and 80 cm^{-3}. Further, from the modeling we find that stimulated amplification of the background H II region continuum radiation contributes significantly to the carbon emission from both components. Strong observational evidence for this result is provided by the close spatial correlation between the C^+ and H II regions.

Finally, we detected emission in sulfur radio recombination lines from both components. We find that the ratios of sulfur-to-carbon line intensities are considerable larger than the [S/C] cosmic abundance ratio and different at different principal quantum numbers, with values in the range between 0.3 and 0.6. We conclude that the large values of the intensity ratios are most likely due to depletion of carbon in the gas phase by a factor of ~ 5, while the observed variation in the intensity ratio with principal quantum number is most likely due to stimulated emission effects in a region of low electron density ($n_e \sim 3$ cm^{-3}) and low temperature ($T_e \sim 50$ K) surrounding the C^+ region.

G. G. gratefully acknowledges support from a Chilean Presidential Science Fellowship and from Fondecyt Project 1950524. This project was partially financed by grants CONACyT-México 4916-E9406, DGAPA-UNAM 102395, and DGAPA-UNAM IN101695. Y. G. also acknowledges partial support from the Third World Academy of Sciences and the ACAL UNESCO Fellowship.

REFERENCES

Brocklehurst, M., & Salem, M. 1977, Comput. Phys. Commun., 13, 39
Brown, R. L., Lockman, F. J., & Knapp, G. R. 1978, ARA&A, 16, 445
Burton, M. G., Hollenbach, D. J., & Tielens, A. G. G. M. 1990, ApJ, 365, 620
Cameron, A. G. W. 1973, Space Sci. Rev. E, 15, 121
Cesaroni, R., Walmsley, C. M., Kömpe, C., & Churchwell, E. 1991, A&A, 252, 278
Chaisson, E. J., Black, J. H., Dupree, A. K., & Cesarsky, D. A. 1972, ApJ, 173, L131
Churchwell, E., Walmsley, C. M., & Cesaroni, R. 1990, A&AS, 83, 119
Draine, B. T., & Bertoldi, F. 1996, ApJ, 468, 269
Dupree, A. K. 1974, ApJ, 187, 25
Dupree, A. K., & Goldberg, L. 1970, ARA&A, 8, 231
Evans, N. J., II, Blair, G. N., Harvey, P., Israel, F., Peters, W. L., III, Scholters, M., De Graaum, T., & Vanden Bout, P. 1981, ApJ, 250, 200
Felli, M., & Harten, R. H. 1981, A&A, 100, 42
Garay, G., Lizano, S., & Gómez, Y. 1994, ApJ, 429, 268 (GLG)
Garay, G., Lizano, S., Gómez, Y., & Brown, R.L. 1998, ApJ, 501, 000
Garay, G., Rodríguez, L. F., Moran, J. M., & Churchwell, E. 1993, ApJ, 418, 368
Gómez, Y., Garay, G., & Lizano, S. 1995, ApJ, 453, 727 (GGL)
Gordon, M. A. 1988, in Galactic and Extragalactic Radio Astronomy, ed. G. L. Verschuur & K. I. Kellermann (Berlin: Springer), 88
Hoang-Binh, D., & Walmsley, C. M. 1974, A&A, 35, 49
Knapp, G. R., Kuiper, T. B. H., & Brown, R. L. 1976, ApJ, 206, 109
Luhman, M. L., Jaffe, D. T., Sternberg, A., Herrmann, F., & Poglitsch, A. 1997, ApJ, 482, 298
Macdonald, G. H., Little, L. T., Brown, A. T., Riley, P. W., Matheson, D. N., & Felli, M. 1981, MNRAS, 195, 387
Morton, D. C. 1974, ApJ, 193, L35
Natta, A., Walmsley, C. M., & Tielens, A. G. G. M. 1994, ApJ, 428, 209
Onello, J. S., & Phillips, J. A. 1995, ApJ, 448, 727
Onello, J. S., Phillips, J. A., Benaglia, P., Goss, W. M., & Terzian, Y. 1994, ApJ, 426, 249
Onello, J. S., Phillips, J. A., & Terzian, Y. 1991, ApJ, 383, 693
Palmer, P., Zuckerman, B., Penfield, H., Lilley, A. E., & Mezger, P. G. 1967, Nature, 215, 40
Pankonin, V. 1980, in Radio Recombination Lines, ed. P. A. Shaver (Dordrecht: Reidel), 111
Pankonin, V., Thomasson, P., & Barshun, J. 1977a, A&A, 54, 335
Pankonin, V., Walmsley, C. M., Wilson, T. L., & Thomasson, P. 1977b, A&A, 57, 341
Plume, R., Jaffe, D. T., & Evans, N. J., II. 1992, ApJS, 78, 505
Roelfsema, P. R., & Goss, W. M. 1991, A&AS, 87, 177
———. 1992, A&A Rev., 4, 161
Roelfsema, P. R., Goss, W. M., & Wilson, T. L. 1987, A&A, 174, 232
Schwab, F. 1980, Proc. SPIE, 231, 18
Silverglate, P. R. 1984, ApJ, 278, 604
Silverglate, P. R., & Terzian, Y. 1978, ApJ, 224, 437
Sofia, U. J, Cardelli, J. A, & Savage, B. D. 1994, ApJ, 430, 650
Spaans, M., & van Dishoeck, E. F. 1997, A&A, 323, 953
Sternberg, A., & Dalgarno, A. 1989, ApJ, 197, 233
Störzer, H., Stutzki, J., & Sternberg, A. 1996, A&A, 310, 592
Tielens, A. G. G. M., & Hollenbach, D. 1985, ApJ, 291, 722
Walmsley, C. M., & Watson, W. D. 1982, ApJ, 260, 317
White, G. J., & Fridlund, C. V. M. 1992, A&A, 266, 452
Wyrowski, F., Schilke, P., Hofner, P., & Walmsley, C. M. 1997, ApJ, 487, L171
Zuckerman, B., & Ball, J. A. 1974, ApJ, 190, 35